Sensors & Actuators: B. Chemical 346 (2021) 130531

Contents lists available at ScienceDirect

Sensors and Actuators: B. Chemical

journal homepage: www.elsevier.com/locate/snb

A dual-signal sensing platform based on nanosheet materials for ratiometric fluorescence and colorimetric detection of enzyme activities in human blood

Yue Zhang [a], Yanhua Wu [b], Lin Liu [a], Wei Wang [a], Wei Zhang [a], Daqian Song [a], Xinghua Wang [a,*], Rui Su [a,*]

[a] College of Chemistry, Jilin University, Changchun, 130012, China
[b] Division of Clinical Research, The First Hospital of Jilin University, Changchun, 130021, China

ARTICLE INFO

Keywords:
Dual-signal sensing
Nanosheet composite
Enzyme
Ratiometric fluorometry
Colorimetry

ABSTRACT

A dual-signal sensing platform comprising g-C_3N_4/MnO_2 nanosheet composite and a routine chromogenic reagent o-phenylenediamine (OPD) was constructed for activity evaluation of several enzymes including Alkaline phosphatase (ALP), acetylcholinesterase (AChE), and butyrylcholinesterase (BChE) in human blood. MnO_2 nanosheets was employed as a catalyst for oxidizing OPD to fluorescent 2,3-diaminophenazine (oxOPD), while g-C_3N_4 nanosheets served as a fluorescent indicator. MnO_2 nanosheets also exhibited inner filter effect (IFE) on the fluorescence of g-C_3N_4 nanosheets due to the overlap of their respective absorption band and fluorescence emission band. Similarly, oxOPD would quench the fluorescence of g-C_3N_4 nanosheets via photoinduced electron transfer (PET) process. By using L-ascorbic acid-2-phosphate (AAP) and acetylthiocholine iodide (ATCh) as substrates, products of target enzyme-catalyzed hydrolysis reactions would reduce MnO_2 nanosheets to Mn^{2+} cations, resulting in the inhibition of OPD oxidation and the fluorescence recovery of g-C_3N_4 nanosheets. Based on these reactions and effects, activities of target enzymes were indicated by the intensity ratio of fluorescence emitted from g-C_3N_4 nanosheets and oxOPD (F_{440}/F_{560}), as well as by the absorbance decrease of oxOPD at 420 nm (ΔA_{420}). Limits of detection (LODs) obtained by the sensing platform for ALP, AChE, and BChE were respectively 0.28 U L^{-1}, 0.19 U L^{-1}, and 0.15 U L^{-1} for ratiometric fluorescence mode, and 1.3 U L^{-1}, 1.0 U L^{-1} and 0.9 U L^{-1} for colorimetric mode. This dual-signal sensing platform can be extended for testing other enzymes after applying appropriate substrates for target enzyme-catalyzed hydrolysis reactions and demonstrates good potential for clinical diagnosis.

1. Introduction

Graphitic-phase carbon nitride (g-C_3N_4) nanosheets as a typical two-dimensional nanometer material possesses a graphite-like structure with Van der Waals interactions between C–N layers [1], which provides it distinguished electronic, optical, mechanical, and thermoelectric properties [2]. Due to its high fluorescence emission ability, g-C_3N_4 nanosheets has been applied to fabricating fluorescent sensors for multiple detections, such as metal ions [3], pesticides [4], and cancer markers [5]. Manganese dioxide (MnO_2) nanosheets is also a two-dimensional nanometer material containing transition metal oxide content [6]. High specific surface area and high valence states of Mn element on the surface of MnO_2 nanosheets endows it with excellent abilities of light absorption, oxidation, and catalysis [7]. By combining g-C_3N_4 nanosheets and MnO_2 nanosheets, a nanocomposite serving as fluorophore, quencher, and catalyst for fluorescent sensing was prepared in this work.

There are many biochemical enzymes in human blood, which play important roles during the metabolic processes of human organisms. Alkaline phosphatase (ALP) is a hydrolase for the dephosphorylation of biochemical substances [8]. The aberrant activity level of ALP in blood indicates a variety of diseases of human body, such as heart failure, worsening renal function, liver dysfunction or damage, and cholestasis [9]. Therefore, sensitive detection of ALP activity in human blood is greatly meaningful for early clinical diagnosis and treatment. As an important family enzyme of glycoprotein hydrolase, cholinesterase commonly present in nervous system, muscle, and red cells of human

* Corresponding author.
E-mail addresses: wxhchem@jlu.edu.cn (X. Wang), sranalchem@163.com (R. Su).

https://doi.org/10.1016/j.snb.2021.130531
Received 8 March 2021; Received in revised form 13 June 2021; Accepted 29 July 2021
Available online 31 July 2021

body for lysing choline-based esters of biochemical molecules. Two variants of cholinesterase, acetylcholinesterase (AChE) and butyrylcholinesterase (BChE) are vital for maintaining normal state of nervous system in human body [10]. So monitoring the activity levels of these cholinesterases in human blood is of great significance in neurobiology, clinical medicine development, and toxicology.

A variety of analytical methods have been developed to detect activities of ALP, AChE, and BChE in biosamples, such as colorimetry [11–13], electrochemistry [14–16], surface-enhanced Raman scattering (SERS) [17–19], fluorometry [20–22], and localized surface plasmon resonance (LSPR) [23,24]. Although these methods provide superior sensitivities than traditional colorimetric methods based on chromogenic substrates such as *p*-Nitrophenyl Phosphate (PNPP) [25] or 5, 5'-dithiobis-(2-nitrobenzoic acid) (DTNB, Ellman's method) [26], highly specific sensing mechanisms of these methods limited their analytical targets and, make their applications for monitoring multi-enzyme activities difficult. In practice, a sensing platform which is capable of providing selective signal responses towards individual targets via universal testing approaches will be more appropriate for application, because it can not only improve the efficiency but also reduce the cost for detecting multiple targets.

Herein, we established a novel sensing strategy as well as a dual-signal sensing platform for activity detections of ALP, AChE, and BChE in human blood by both ratiometric fluorometry and colorimetry. The sensing mechanism of the present strategy was illustrated in Scheme 1. Briefly, MnO_2 nanosheets suppressed the violet fluorescence emitted from g-C_3N_4 nanosheets (440 nm) via inner filter effect (IFE) and catalyzed the oxidation of *o*-phenylenediamine (OPD). The product of the oxidation reaction, 2,3-diaminophenazine (oxOPD), emitted orange fluorescence (560 nm) and quenched the emission of g-C_3N_4 nanosheets via photoinduced electron transfer (PET) process. By respectively using L-ascorbic acid-2-phosphate (AAP) and acetylthiocholine iodide (ATCh) as substrates for the respective hydrolysis reactions under catalysis of ALP and AChE or BChE, ascorbic acid (AA) and thiocholine (TCh) were produced efficiently. Both AA and TCh had the capacity to reduce MnO_2 nanosheets to Mn^{2+}, therefore the absorption of oxOPD (420 nm) and the fluorescence emitted from oxOPD and g-C_3N_4 nanosheets in this sensing system were all determined by activities of the target enzyme. By respectively employing the intensity ratio of fluorescence emitted from g-C_3N_4 nanosheets to that from oxOPD (F_{440}/F_{560}) and the absorbance decrease of oxOPD at 420 nm (ΔA_{420}) as the fluorescent and colorimetric response signals, a selective and sensitive strategy was proposed for separately detecting activities of ALP, AChE and BChE in human whole blood samples. The proposed strategy exhibited excellent analytical performance and universality, suggesting its good potential for future applications in clinical diagnosis.

2. Experimental

2.1. Materials and instruments

Melamine, Sodium orthovanadate (Na_3VO_4) and uric acid (UA) were purchased from Shanghai Macklin Biochemical Co.,Ltd. *o*-Phenylenediamine (OPD), Tetramethylammonium hydroxide (TMA·OH), L-ascorbic acid-2-phosphate (AAP), donepezil HCl, glucose (Glu), glutathione (GSH), Isoleucine (Ile), aspartic acid (Asp), serine (Ser), glycine (Gly), and arginine (Arg) were purchased from Shanghai Aladdin Chemistry Company Ltd. H_2O_2, $MnCl_2{\cdot}4H_2O$, $CaCl_2$, $ZnCl_2$, $MgCl_2$ and methanol were purchased from Beijing Chemical Works. Alkaline phosphate (ALP) from calf intestinal mucosa (10,000 U mL^{-1}) was provided by Beijing New England Biolabs. Acetylcholinesterase (AChE) from fly head, butyrylcholinesterase (BChE) from horse serum, acetylthiocholine iodide (ATCh), glucose (Glu), tyrosine (Tyr), L-cysteine (Cys), human serum albumin (HSA), trypsin, and transglutaminase (TG) were purchased from Shanghai Yuanye Bio-Technology Co., Ltd. The anticoagulant whole blood samples from three healthy volunteers, and the corresponding plasma and erythrocyte samples were prepared by the First Hospital of Jilin University.

Fluorescence spectra were recorded on an F-7000 spectrofluorophotometer (HITACHI Co., Ltd., Japan). Ultraviolet-visual absorption (UV-Vis) spectra were collected with a Cary 60 UV-Vis spectrometer (Agilent Technologies Inc., USA). A 1-cm quartz cuvette was used in all experiments. Morphology of nanosheet materials was observed on a Tecnai F20 transmission electron microscopy (TEM, Thermo Fisher Scientific, Dutch) operated at 200 kV. Thicknesses of nanosheet materials were evaluated by an atomic force microscope system (AFM, Dimension Icon with ScanAsyst, Bruker Co., Germany) in air mode. X-ray photoelectron spectroscopy (XPS) profiles were obtained on an ESCALAB 250 spectrometer (Thermo Fisher Scientific, USA) by using a monochromatic X-ray source with Al Kα excitation

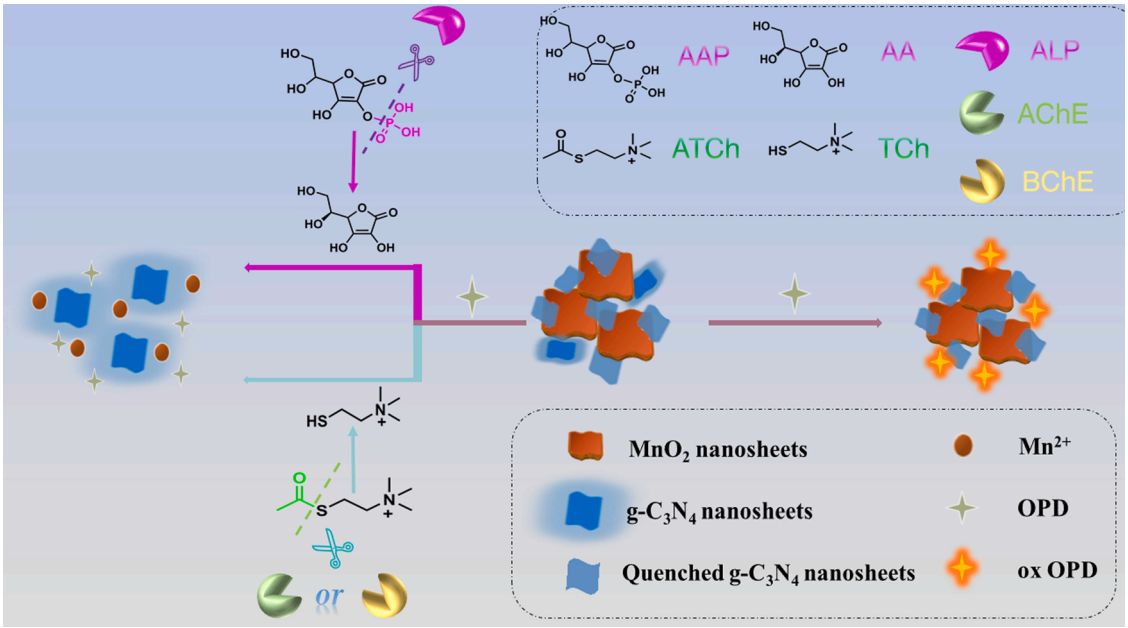

Scheme 1. Schematic illustration of the proposed sensing strategy.

(1486.6 eV). Mid-infrared absorption spectrum was recorded using KBr pellet on a Nicolet IS5 Fourier transform spectrophotometer (FT-IR, Thermo Fisher Scientific, USA) in a wavenumber range of 4000 ~ 400 cm^{-1}. Deionized water (18.2 MΩ cm) was obtained from a GBW purification system (Beijing Purkinje General Instrument Co, China). All pH values were measured with a PHS-3C pH-Meter (INESA Scientific Inc., China). Zeta potentials were measured via photon correlation spectroscopy (PCS) on a Nano ZS90 laser particle analyzer (Malvern Instruments, UK) at room temperature.

2.2. Activity detection of enzymes in buffer

A standard enzyme solution (50 μL) of ALP, AChE or BChE at a certain activity level was added into PBS buffer (580 μL, 10 mM, pH 7.4) containing the corresponding substrate (AAP or ATCh, 1 mM). Then the mixed solution was incubated for 30 min. Next, 100 μL of g-C_3N_4 nanosheets and 120 μL of MnO_2 nanosheets were added into the mixed solution followed by another incubation for 15 min. After that, OPD solution (100 μL, 10 mM) was added and the mixed solution was incubated again for 60 min. Finally, fluorescence spectrum under excitation at 370 nm and UV-Vis absorption spectra in the wavelength range of 300 ~ 600 nm were recorded. All incubations were performed at 37 ℃.

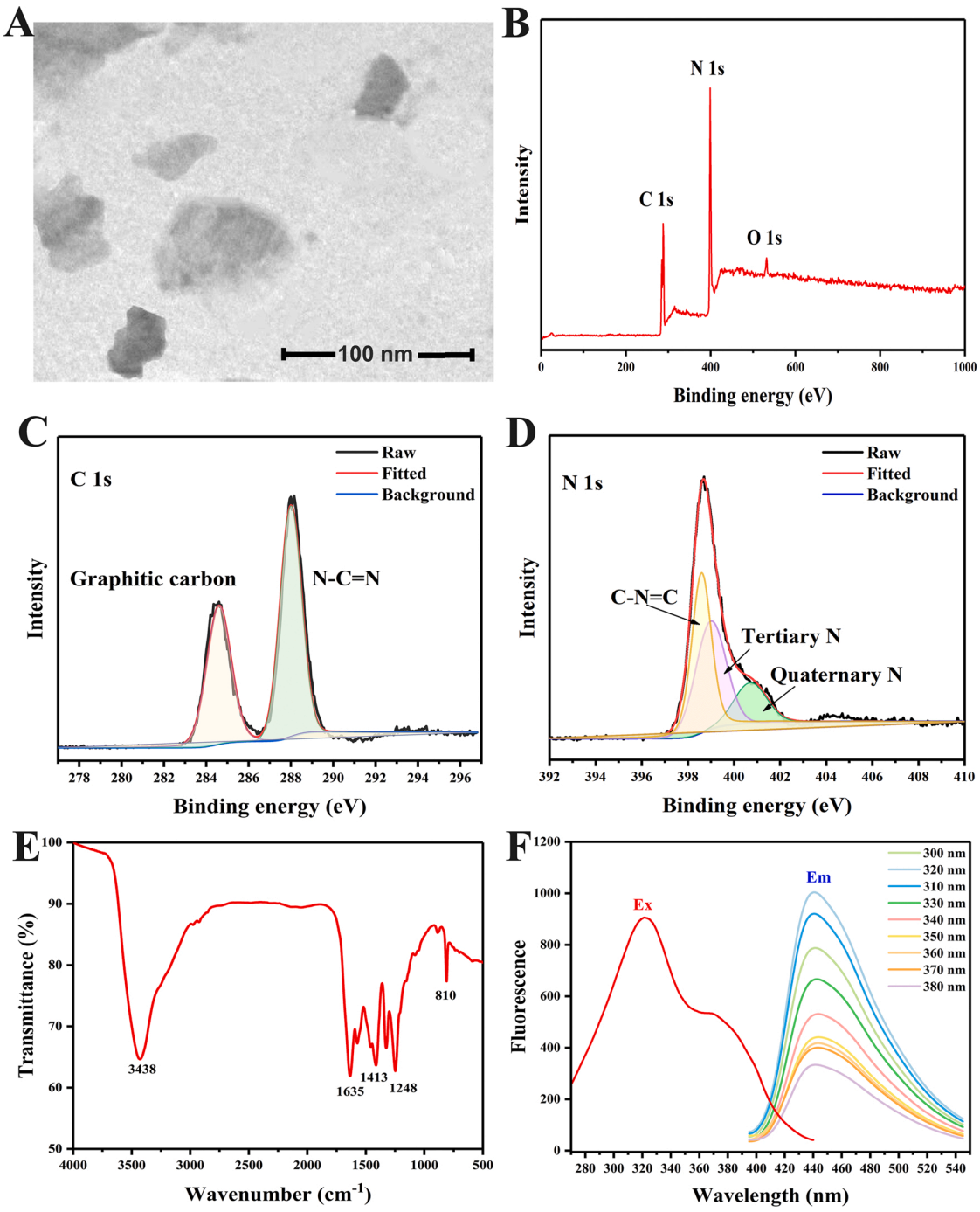

Fig. 1. Characterization of g-C_3N_4 nanosheets. (A) TEM image, (B) XPS full-scan survey, and high-resolution scans of (C) C1 s and (D) N1 s, (E) FT-IR absorption spectrum, (F) fluorescence excitation spectrum and fluorescence emission spectra under various excitation wavelengths (300 nm ~ 380 nm).

2.3. Detection of enzyme inhibitors

For detecting inhibitors, 50 μL of Na_3VO_4, donepezil, and bambuterol solutions with different concentrations were correspondingly added into 580 μL of PBS buffers containing ALP (200 U L^{-1}), AChE (10 U L^{-1}), and BChE (24 U L^{-1}), followed by gently shaking for 20 min. Then, 50 μL of AAP (20 mM, for ALP) or 50 μL of ATCh (20 mM, for AChE or BChE) were added into corresponding solutions. The solutions were incubated at 37 ℃ for 30 min. The subsequent measuring procedures are the same as those for the detection of enzymes performed in Section 2.2.

2.4. Activity detection of enzymes in human whole blood

All human whole blood samples and their derivated plasma and erythrocyte samples were diluted with PBS buffer (10 mM, pH 7.4) prior to assay. The dilution ratios of samples were as follows: ALP assay in whole blood, 300-fold; ALP assay in plasma, 100-fold; AChE assay in whole blood or erythrocyte, 4000-fold; BChE assay in whole blood or plasma, 4000-fold. In addition, 50 μL of bambuterol (1 mM) was used to inhibit the activity of BChE prior to AChE assay, and 50 μL of donepezil (1 mM) was used to inhibit the activity of AChE prior to BChE assay. The following steps of each assay were the same as those performed in Section 2.2.

3. Results and discussion

3.1. Characterization of g-C_3N_4/ MnO_2 nanosheets

Preparation procedures of g-C_3N_4 nanosheets and MnO_2 nanosheets were listed in Supplementary Information. TEM image (Fig. 1A) demonstrates the ultrathin two-dimensional structure of g-C_3N_4 nanosheets. AFM image (Fig. S1A) and corresponding height profile (Fig. S1B) confirm that the thickness of g-C_3N_4 nanosheets is about 2.6 nm. XPS characterization (Fig. 1B) indicates that there are three main types of elements (C, N, and O) in g-C_3N_4 nanosheets. As shown in Fig. 1C, C 1s spectrum can be divided into two peaks at 284.6 eV and 288.0 eV, which are assigned to the graphitic carbon and N–C=N from the triazine ring (C_3N_3) or heptazine (C_6N_7) units, respectively. N 1s spectrum (Fig. 1D) reveals the three types of N atoms in g-C_3N_4 nanosheets, including C–N = C (398.4 eV), tertiary N (398.8 eV), and quaternary N (400.6 eV) [27, 28]. Chemical groups on g-C_3N_4 nanosheets were further examined by FT-IR spectroscopy (Fig. 1E). The obvious absorption band at 810 cm^{-1} is ascribed to the vibration of triazine ring, the narrow absorption bands between 1248 cm^{-1} to 1635 cm^{-1} are originated by the vibrations of C–N and C = N groups, and the wider absorption band at 3438 cm^{-1} is consistent with N-H stretching and hydrogen-bonding interactions [1]. As depicted in Fig. 1F, the fluorescence peak excitation and emission wavelengths are 320 nm and 440 nm, respectively. The fluorescence peak emission wavelength of g-C_3N_4 nanosheets shows no obvious shift along with the variation of excitation wavelength from 300 nm to 380 nm.

Fig. 1

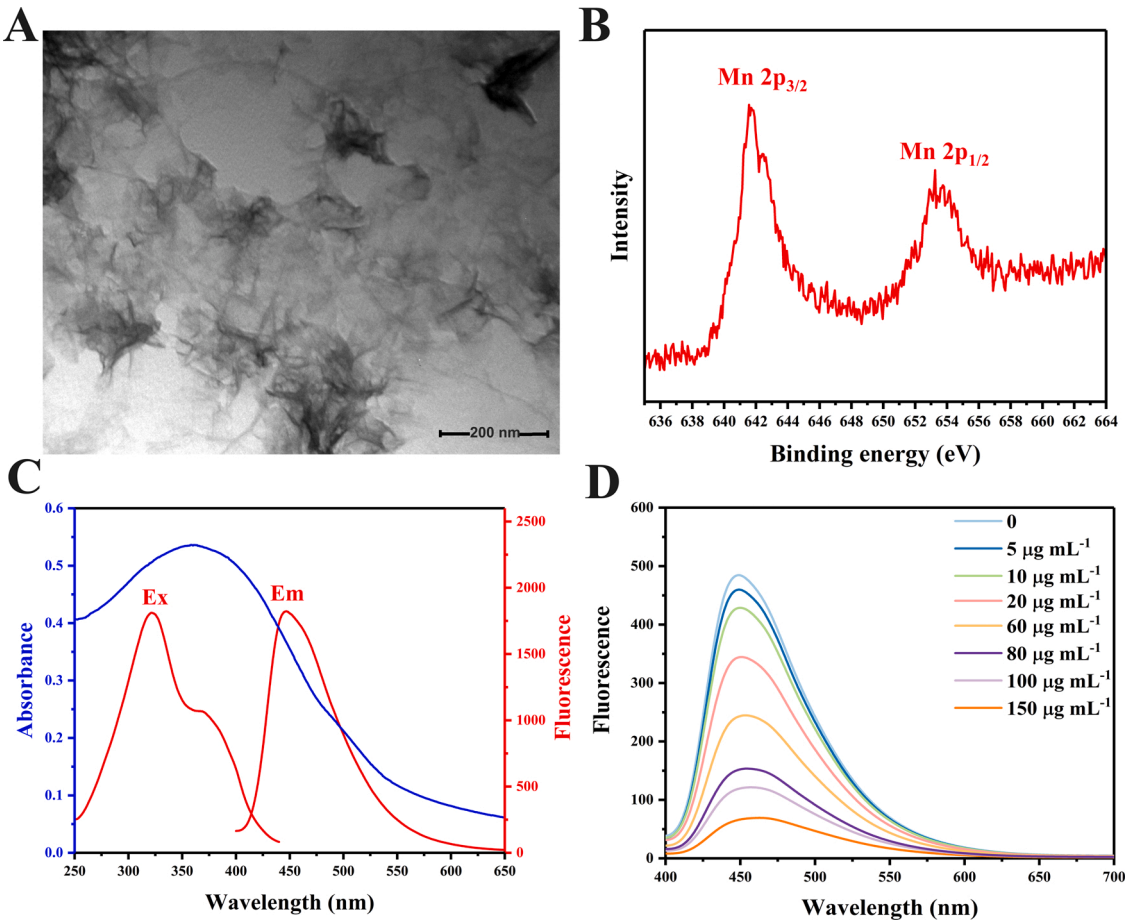

Fig. 2. Morphology of MnO_2 nanosheets and its influence on fluorescence of g-C_3N_4 nanosheets. (A) TEM image, (B) XPS spectrum, (C) overlap between UV-Vis absorption spectrum of MnO_2 nanosheets and fluorescence excitation or emission spectra of g-C_3N_4 nanosheets, (D) influence of MnO_2 nanosheets concentration on fluorescence emission of g-C_3N_4 nanosheets (Concentration of g-C_3N_4 nanosheets, 200 μg mL^{-1}).

MnO_2 nanosheets also exhibits a two-dimensional sheet structure with a large surface area (Fig. 2A), that can provide abundant active sites for catalytic oxidation of OPD. AFM image (Fig. S2 A) and corresponding height profile (Fig. S2 B) indicate that as-prepared MnO_2 presented a polycrystalline sheet structure, with a thickness of about 1.7 nm. As presented in Fig. 2B, the XPS peaks of Mn $2p_{3/2}$ and Mn $2p_{1/2}$ are centered at about 641.9 eV and 653.6 eV, respectively, with a spin-energy separation of 11.7 eV, which confirms the formation of Mn(IV) O_2 nanosheets [29,30]. Fig. 2C illustrates the UV-Vis absorption spectrum of MnO_2 nanosheets and the fluorescence excitation and emission spectra of g-C_3N_4 nanosheets. The obvious overlap between the UV-Vis absorption spectrum and the fluorescence excitation or emission spectrum implied the possibility of MnO_2 nanosheets-induced IFE on the fluorescence of g-C_3N_4 nanosheets.

3.2. Sensing mechanism

As shown in Fig. 2D, after simply mixing MnO_2 nanosheets and g-C_3N_4 nanosheets at various ratios to obtain nanocomposites, the fluorescence intensity of g-C_3N_4 nanosheets gradually decreases along with the increasing amount of MnO_2 nanosheets, demonstrating the fluorescence quenching ability of MnO_2. Fig. S3 illustrates the fluorescence

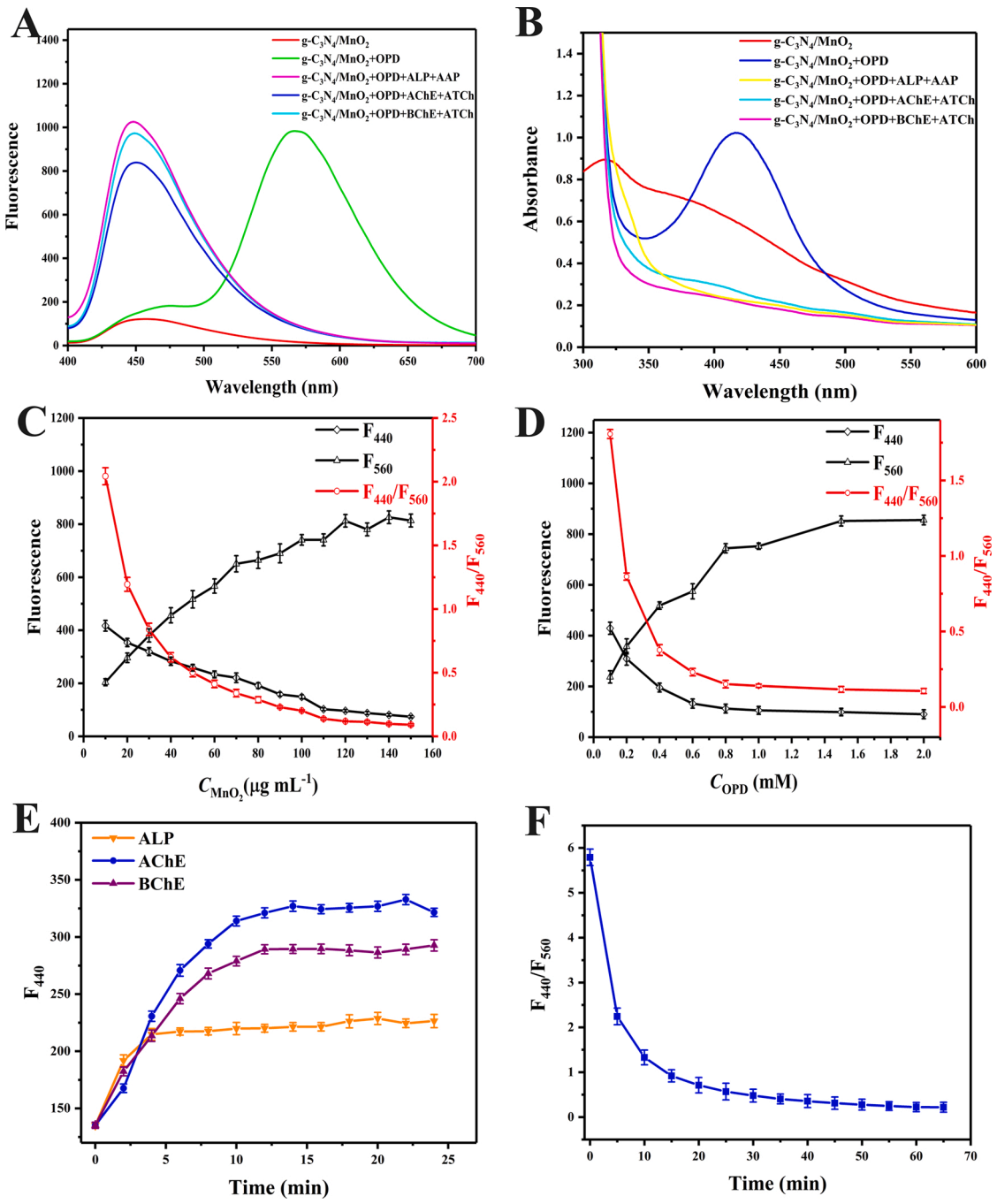

Fig. 3. (A) Fluorescence spectra and (B) UV-Vis absorption spectra of testing systems containing target enzymes and different testing reagents. Concentrations of g-C_3N_4 nanosheets, MnO_2 nanosheets, OPD, ALP, AChE, BChE, AAP, ATCh were 200 μg mL^{-1}, 120 μg mL^{-1}, 1 mM, 200 U L^{-1}, 100 U L^{-1}, 100 U L^{-1}, 1 mM, 1 mM, respectively. (C) Effect of concentration of MnO_2 nanosheets on fluorescence response. (D) Effect of concentration of OPD on fluorescence response. (E) Effect of incubation time for target enzyme-catalyzed hydrolysis and (F) for OPD oxidation on fluorescence response.

decay curves of g-C_3N_4 nanosheets in absence and presence of MnO_2 nanosheets and OPD. By fitting these decay curves to second-order exponential functions, the fluorescence lifetime values of g-C_3N_4 nanosheets, g-C_3N_4/MnO_2 nanocomposite, and g-C_3N_4/MnO_2 nanocomposite with OPD were calculated as 5.44 ns, 5.85 ns, and 4.11 ns, respectively. The negligible variation of the fluorescence lifetime values obtained by testing g-C_3N_4 nanosheets and g-C_3N_4/MnO_2 nanocomposite suggests the dynamic quenching effect (DQE) is not obvious during the fluorescence quenching process of MnO_2 nanosheets on g-C_3N_4 nanosheets, since DQE usually results in the obvious decrease of fluorescence lifetime of a fluorophore. Zeta potentials of g-C_3N_4 nanosheets, MnO_2 nanosheets and g-C_3N_4/MnO_2 nanocomposite in PBS buffer (pH = 7.4, 10 mM) were measured and the results (Fig. S4) indicated the negative surface charge nature of both g-C_3N_4 nanosheets and MnO_2 nanosheets, which are consistent with previous reports [31–33]. Due to the chemical inertness of g-C_3N_4 nanosheets as well as the repulsion effect among negatively charged surfaces of these nanosheets, chemical reaction or complexation can hardly occur between g-C_3N_4 nanosheets and MnO_2 nanosheets, therefore the contribution of static quenching effect (SQE) for the above fluorescence quenching process is very little. According to the overlap between the UV-Vis absorption spectrum of MnO_2 nanosheets and the fluorescence spectra of g-C_3N_4 nanosheets (Fig. 2C), it can be concluded that the IFE of MnO_2 nanosheets on the fluorescence of g-C_3N_4 nanosheets plays a key role during the above fluorescence quenching process.

As illustrated in Fig. 3A, ALP or cholinesterase-catalyzed hydrolysis reactions on AAP or ATCh resulted in decreasing fluorescence of oxOPD at 560 nm, which was ascribed to the inhibited oxidation of OPD, since products of these hydrolysis reactions, AA and TCh, both possess enough reducibility to reduce MnO_2 nanosheets serving as the catalyst of the oxidation of OPD. As a typical electron-acceptor molecule containing benzene ring, amide groups, and a large conjugated π-system, oxOPD can be easily immobilized on the surface of g-C_3N_4 nanosheets through hydrogen bonding and π–π stacking, resulting in the quenching of the fluorescence emission at 440 nm via PET process [34]. The obvious variation between the fluorescence lifetime values of g-C_3N_4/MnO_2 nanocomposite with and without the oxidation of OPD (Fig. S3) revealed this PET-quenching process occurred efficiently. Therefore, after the above hydrolysis reactions, both the restricted IFE of MnO_2 nanosheets and the inhibited oxidation of OPD would lead to the fluorescence recovery of g-C_3N_4 nanosheets at 440 nm, similarly the inhibited oxidation of OPD would induce the fluorescence decrease of oxOPD at 560 nm (Fig. 3A). By using the intensity ratio of fluorescence at 440 nm to that at 560 nm (F_{440}/F_{560}) as the response signal, a sensitive ratiometric fluorescence strategy for activity evaluations of three target enzymes was established based on the above mechanism. To obtain good fluorescence excitation efficiencies for both g-C_3N_4 nanosheets and oxOPD, 370 nm was finally selected as the excitation wavelength for this sensing strategy.

Similarly, the absorbance change of oxOPD at 420 nm (ΔA_{420}) induced by the variation of oxOPD amount before and after a certain target enzyme-catalyzed hydrolysis reaction (Fig. 3B) was employed as another response signal to establish a colorimetric strategy for activity evaluation of the target enzyme. Here the value of ΔA_{420} was calculated according to the following equation,

$$\Delta A_{420} = A - A_0$$

where A_0 and A are the peak absorbance values of oxOPD (420 nm) obtained before and after the target enzyme-catalyzed hydrolysis reaction, respectively.

3.3. Optimization of assay conditions

Several vital experimental conditions for the present sensing strategy were optimized to obtain the best analytical performance. Before optimizing, the amount of g-C_3N_4 nanosheets used as a fluorescent indicator was set as 100 μL to provide sufficient fluorescence emission during sensing procedure. Effect of initial concentrations of MnO_2 nanosheets and OPD on the fluorescence response signal F_{440}/F_{560} were investigated, and the results were illustrated in Fig. 3C and D respectively. Since oxOPD was generated by the MnO_2 nanosheets-catalyzed oxidation of OPD, increasing the initial amount of MnO_2 nanosheets or OPD would both lead to the increase of fluorescence emission of oxOPD (F_{560}) as well as the oxOPD-induced PET quenching of fluorescence emitted from g-C_3N_4 nanosheets (F_{440}), resulting in the continuous decrease of fluorescence intensity ratio F_{440}/F_{560}. Moreover, increasing the initial amount of MnO_2 nanosheets would also enhance the IFE quenching on fluorescence emitted from g-C_3N_4 nanosheets (F_{440}). According to these results, the initial concentration of MnO_2 nanosheets and OPD were respectively chosen to be 120 μg mL^{-1} and 1 μM for further assay. Fig. 3E indicates fluorescence intensities of g-C_3N_4 would be restored by the target enzyme-catalyzed hydrolysis reactions and all these reactions reached their equilibrium in 15 min. Fig. 3F shows the reaction of OPD oxidation finished in 60 min. Because the pH value of human blood and temperature of human body are commonly maintained closed to 7.4 and 37 ℃, PBS (pH = 7.4, 10 mM) was selected as the buffer for testing, and the incubation temperature for all reactions was set at 37 ℃ [13,35,36]. In summary, the optimal detection conditions of the sensing system are as follows: amounts of g-C_3N_4 nanosheets and MnO_2 nanosheets: 100 μL and 120 μL, respectively; incubation time for each hydrolysis reaction and OPD oxidation: 15 min and 60 min. respectively.

3.4. Selectivity

We further investigated the potential interference of several substances commonly coexisted in human blood, including Ca^{2+}, Mg^{2+}, Mn^{2+}, Zn^{2+}, UA, Cys, Ile, Asp, Ser, Gly, Arg, Phe, GSH, Tyr, Trypsin, Glu, TG, and HSA, on the present sensing strategy. As illustrated in Fig. S5, these substances exhibited negligible fluorescence or absorption responses, indicating the good selectivity of the present sensing strategy.

3.5. Analytical performance

Fluorescence responses of this sensing system towards activities of target enzymes were exhibited in Fig. 4A, C, and E. Linear ranges for activity detection of ALP, AChE and BChE are 0.5 ~ 20 U L^{-1} (Fig. 4B), 0.5 ~ 9 U L^{-1} (Fig. 4D) and 0.2 ~ 10 U L^{-1} (Fig. 4F), respectively. Limits of detections (LODs: 3 S/m) for ALP, AChE, and BChE were calculated as 0.28 U L^{-1}, 0.19 U L^{-1}, and 0.15 U L^{-1} by the ratiometric fluorescence mode, respectively.

Similarly, absorption responses of this sensing system towards activities of target enzymes were shown in Fig. 5A, C, and E. The absorbance decrease ΔA_{420} show linear relationships with activities of ALP, AChE, and BChE in the ranges of 1 ~ 50 U L^{-1} (Fig. 5B), 2 ~ 30 U L^{-1} (Fig. 5D), and 1 ~ 40 U L^{-1} (Fig. 5F), respectively. LODs for ALP, AChE, and BChE obtained by the colorimetric mode are 1.3 U L^{-1}, 1.0 U L^{-1}, and 0.9 U L^{-1}, respectively.

Analytical performance of this sensing strategy was compared with that of previously reported methods (Table S1). Results indicated that this sensing strategy has excellent sensitivity for detection of ALP, AChE, and BChE.

3.6. Inhibition assessment for the enzymes

To further verify the ability of the sensing platform for screening the above inhibitors, the 50% inhibiting concentration (IC_{50}) of these inhibitors were examined by both colorimetric and fluorescence detection mode. As illustrated in Fig. S6, the obtained IC_{50} values are similar to those reported previously [37–39].

3.7. Application to real samples

Three real whole blood samples and their derivated plasma and

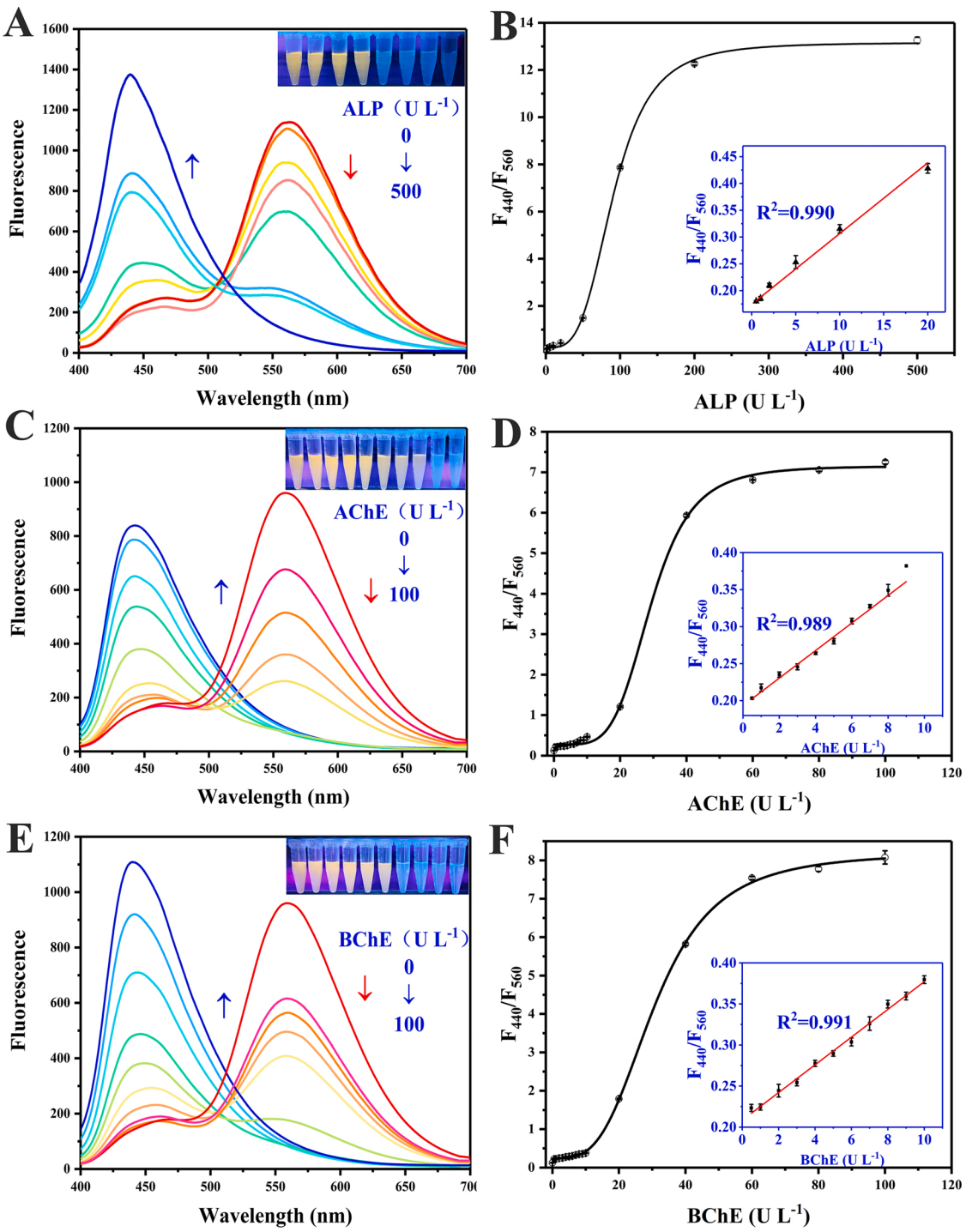

Fig. 4. Fluorescence response of the sensing system towards ALP (A and B), AChE (C and D), and BChE (E and F). Insets in A, C, and E: photographs of the sensing system under illumination at 365 nm. Insets in B, D, and F: linear relationships between fluorescence intensity ratio F_{440}/F_{560} and activities of corresponding enzymes.

erythrocyte samples were examined by the present sensing strategy. The p-Nitrophenyl Phosphate (PNPP) method [25] (for ALP) and the Ellman's method [26] (for AChE or BChE after inhibition of another cholinesterase prior to testing) were employed as reference methods. Due to the color interference arose from erythrocyte, only the derivated plasma samples were examined by the colorimetric mode of the present sensing strategy. Results listed in Table S2 demonstrated the good accuracy, precision, and applicability of the present sensing strategy.

4. Conclusion

In this work, a dual-signal sensing platform was developed based on g-C_3N_4/MnO_2 nanosheet composites and OPD for selective and sensitive activity detections of ALP, AChE, and BChE in human blood. By respectively using chemically inert g-C_3N_4 nanosheets and reductive OPD as the fluorescent indicator and the chromogenic development reagent, amount variation of catalytic MnO_2 nanosheets, which was determined by the reduction reaction induced by the product of a target enzyme-catalyzed hydrolysis reaction of the corresponding substrate,

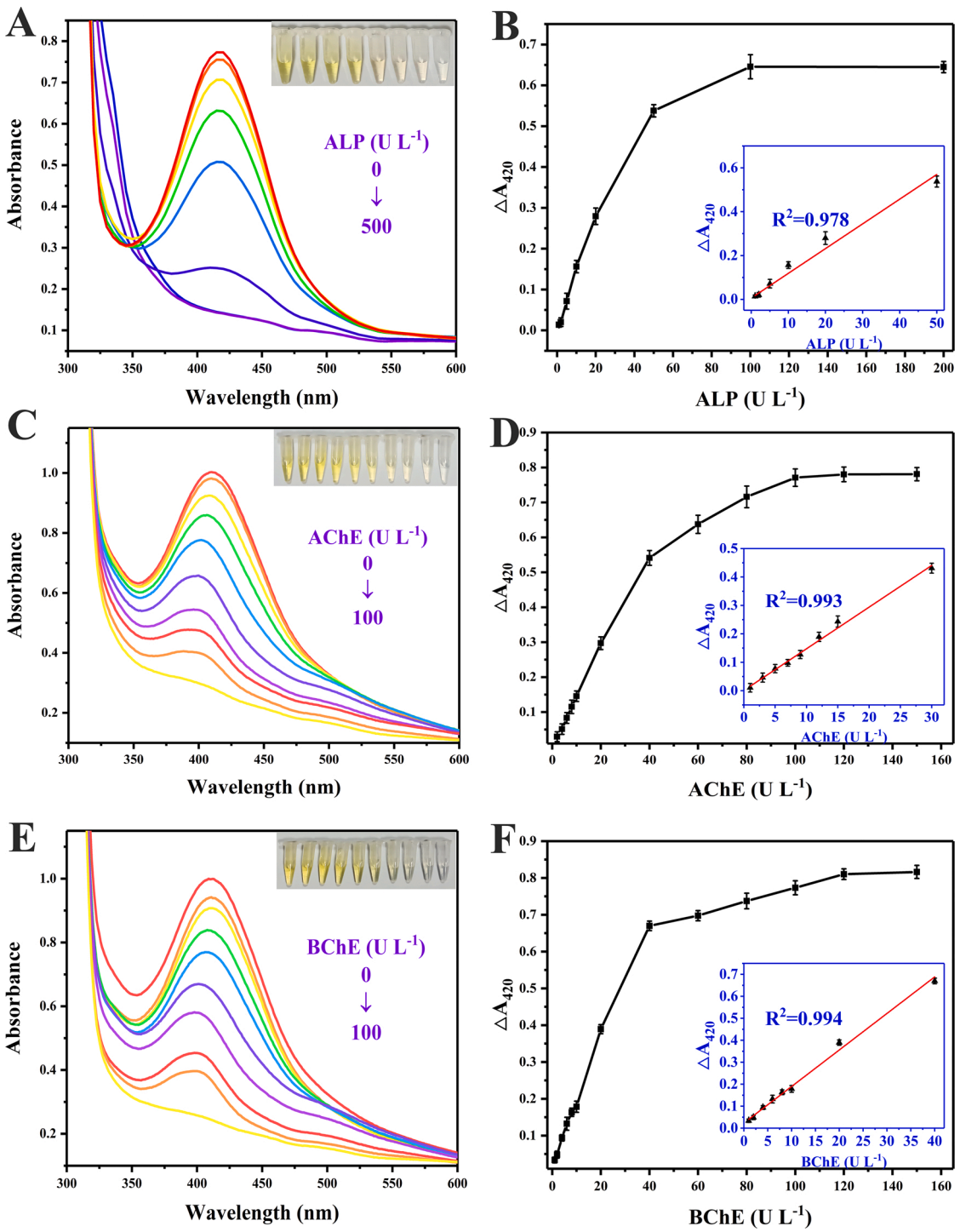

Fig. 5. UV-Vis absorption response of the sensing system towards ALP (A and B), AChE (C and D), and BChE (E and F). Insets in A, C, and E: photographs of the sensing system under visible light. Insets in B, D, and F: linear relationships between absorbance decrease ΔA_{420} and activities of corresponding enzymes.

resulted in the spectral response of the sensing system towards activity of the target enzyme. Absorbance of oxOPD (the oxidized OPD), as well as intensity ratio of fluorescence emission of g-C_3N_4 nanosheets to that of oxOPD, were employed as response signals to realized the colorimetric and the ratiometric fluorescence detection modes. Good analytical performance and reliable detection results obtained by testing real samples indicate the excellent applicability of the present strategy. The developed dual-signal sensing platform can be easily applied to the detection of other biosubstances involved in generating products for inhibiting MnO_2 nanosheets-catalyzed oxidation of OPD, which provides a potential for developing new sensing strategies in clinical diagnosis.

CRediT authorship contribution statement

Yue Zhang: Conceptualization, Data curation, Methodology, Software, Writing - original draft. **Yanhua Wu:** Supervision, Investigation, Formal analysis, Writing - review & editing. **Lin Liu:** Data curation, Methodology, Writing - review & editing. **Wei Wang:** Methodology, Formal analysis, Writing - review & editing. **Wei Zhang:** Methodology,

Formal analysis, Writing - review & editing. **Daqian Song:** Writing - review & editing. **Xinghua Wang:** Funding acquisition, Project administration, Supervision, Resources, Writing - review & editing. **Rui Su:** Supervison, Writing - review & editing.

Declaration of Competing Interest

The authors report no declarations of interest.

Acknowledgements

This work was supported by the Industrialization Project of Education Department of Jilin Province (No. JJKH20200944KJ), the National Natural Science Foundation of China (No. 82004005), the Fundamental Research Funds for the Central Universities of China, and the Training Program of Excellent Young Teachers of Jilin University.

Appendix A. Supplementary data

Supplementary material related to this article can be found, in the online version, at doi:https://doi.org/10.1016/j.snb.2021.130531.

References

[1] X.D. Zhang, X. Xie, H. Wang, J.J. Zhang, B.C. Pan, Y. Xie, Enhanced Photoresponsive Ultrathin Graphitic-Phase C_3N_4 Nanosheets for Bioimaging, J. Am. Chem. Soc. 135 (2013) 18–21.
[2] Y.Z. Yu, Q. Zhou, J.G. Wang, The ultra-rapid synthesis of 2D graphitic carbon nitride nanosheets via direct microwave heating for field emission, Chem Commun 52 (2016) 3396–3399.
[3] J. Tian, Q. Liu, A.M. Asiri, A.O. Al-Youbi, X. Sun, Ultrathin graphitic carbon nitride nanosheet: a highly efficient fluorosensor for rapid, ultrasensitive detection of Cu^{2+}, Anal. Chem. 85 (2013) 5595–5599.
[4] H. Mei, H. Shu, M. Lv, W. Liu, X. Wang, Fluorescent assay based on phenyl-modified g-C_3N_4 nanosheets for determination of thiram, Mikrochim. Acta 187 (2020) 159.
[5] B. Huang, X.P. Liu, J.S. Chen, C.J. Mao, H.L. Niu, B.K. Jin, Electrochemiluminescence immunoassay for the prostate-specific antigen by using a CdS/chitosan/g-C_3N_4 nanocomposite, Mikrochim. Acta 187 (2020) 155.
[6] K. Kai, Y. Yoshida, H. Kageyama, G. Saito, T. Ishigaki, Y. Furukawa, et al., Room-temperature synthesis of manganese oxide monosheets, J. Am. Chem. Soc. 130 (2008) 15938–15943.
[7] C. Peng, H. Xing, X. Fan, Y. Xue, J. Li, E. Wang, Glutathione regulated inner filter effect of MnO_2 nanosheets on boron nitride quantum dots for sensitive assay, Anal. Chem. 91 (2019) 5762–5767.
[8] J.E. Coleman, Structure and mechanism of alkaline phosphatase, Annu. Rev. Biophys. Biomol.Struct. 21 (1992) 441–483.
[9] G.M. Carman, G.-S. Han, Roles of phosphatidate phosphatase enzymes in lipid metabolism, Trends Biochem. Sci 31 (2006) 694–699.
[10] M. Pohanka, Inhibitors of acetylcholinesterase and butyrylcholinesterase meet immunity, Int J Mol Sci 15 (2014) 9809–9825.
[11] D. Shi, Y. Sun, L. Lin, C. Shi, G. Wang, X. Zhang, Naked-eye sensitive detection of alkaline phosphatase (ALP) and pyrophosphate (PPi) based on a horseradish peroxidase catalytic colorimetric system with Cu(II), Analyst 141 (2016) 5549–5554.
[12] Y. Li, H. Bai, C. Li, G. Shi, Colorimetric Assays for acetylcholinesterase activity and inhibitor screening based on the disassembly-assembly of a water-soluble polythiophene derivative, Acs Applied Materials & Interfaces 3 (2011) 1306–1310.
[13] X. Wang, K. Koh, H. Chen, Colorimetric assay of butyrylcholinesterase activity based on para-sulfonatocalix 4 arene-modified gold nanoparticles, Sens. Actuators, B 251 (2017) 869–876.
[14] H. Jiang, X. Wang, Alkaline phosphatase-responsive anodic electrochemiluminescence of CdSe nanoparticles, Anal. Chem. 84 (2012) 6986–6993.
[15] Y. Panraksa, W. Siangproh, T. Khampieng, O. Chailapakul, A. Apilux, Paper-based amperometric sensor for determination of acetylcholinesterase using screen-printed graphene electrode, Talanta 178 (2018) 1017–1023.
[16] M. Pohanka, Voltammetric assay of butyrylcholinesterase in plasma samples and its comparison to the standard spectrophotometric test, Talanta 119 (2014) 412–416.
[17] N. Li, H. Chen, M. Zhang, Y. Zha, Z. Mu, Y. Ma, et al., A universal ultrasensitive platform for enzyme-linked immunoassay based on responsive surface-enhanced Raman scattering, Sens. Actuators, B 315 (2020).
[18] Z. Liron, A. Zifman, V. Heleg-Shabtai, Surface-enhanced Raman scattering detection of cholinesterase inhibitors, Anal. Chim. Acta. 703 (2011) 234–238.
[19] N. Nechaeva, T. Prokopkina, G. Makhaeva, E. Rudakova, N. Boltneva, C. Dishovsky, et al., Quantitative butyrylcholinesterase activity detection by surface-enhanced Raman spectroscopy, Sens. Actuators, B 259 (2018) 75–82.
[20] S.-J. Li, C.-Y. Li, Y.-F. Li, J. Fei, P. Wu, B. Yang, et al., Facile and sensitive near-Infrared fluorescence probe for the detection of endogenous alkaline phosphatase activity In Vivo, Anal. Chem. 89 (2017) 6854–6860.
[21] Z. Qian, L. Chai, C. Tang, Y. Huang, J. Chen, H. Feng, A fluorometric assay for acetylcholinesterase activity and inhibitor screening with carbon quantum dots, Sens. Actuators, B 222 (2016) 879–886.
[22] G. Chen, H. Feng, X. Jiang, J. Xu, S. Pan, Z. Qian, Redox-controlled fluorescent nanoswitch based on reversible disulfide and its application in butyrylcholinesterase activity assay, Anal. Chem. 90 (2018) 1643–1651.
[23] F. Wang, Y. Li, Y. Han, Z. Ye, L. Wei, H.-B. Luo, et al., Single-particle enzyme activity assay with spectral-resolved dark-field optical microscopy, Anal. Chem. 91 (2019) 6329–6339.
[24] T.-J. Lin, K.-T. Huang, C.-Y. Liu, Determination of organophosphorous pesticides by a novel biosensor based on localized surface plasmon resonance, Biosens. Bioelectron. 22 (2006) 513–518.
[25] O.A. Bessey, O.H. Lowry, M.J. Brock, A method for the rapid determination of alkaline phosphates with five cubic millimeters of serum, J. Biol. Chem. 164 (1946) 321–329.
[26] G.L. Ellman, K.D. Courtney, V. Andres Jr., R.M. Feather-Stone, A new and rapid colorimetric determination of acetylcholinesterase activity, Biochem. Pharmacol. 7 (1961) 88–95.
[27] A. Afkhami, P. Hashemi, H. Bagheri, J. Salimian, A. Ahmadi, T. Madrakian, Impedimetric immunosensor for the label-free and direct detection of botulinum neurotoxin serotype A using Au nanoparticles/graphene-chitosan composite, Biosens. Bioelectron. 93 (2017) 124–131.
[28] Q.X. Guo, Y. Xie, X.J. Wang, S.Y. Zhang, T. Hou, S.C. Lv, Synthesis of carbon nitride nanotubes with the C_3N_4 stoichiometry via a benzene-thermal process at low temperatures, Chem. Commun. (2004) 26–27.
[29] M. Toupin, T. Brousse, D. Belanger, Charge storage mechanism of MnO_2 electrode used in aqueous electrochemical capacitor, Chem. Mater. 16 (2004) 3184–3190.
[30] W. Fan, W. Bu, B. Shen, Q. He, Z. Cui, Y. Liu, et al., Intelligent MnO_2 nanosheets anchored with upconversion nanoprobes for concurrent pH-H_2O_2-responsive UCL imaging and oxygen-elevated synergetic therapy, Adv. Mater. 27 (2015) 4155–4161.
[31] G. Liu, X. Qiao, M.A. Gondal, Y. Liu, K. Shen, Q. Xu, Comparative study of pure g-C_3N_4 and sulfur-doped g-C_3N_4 catalyst performance in photo-degradation of persistent pollutant under visible light, J Nanosci Nanotechnol. 18 (2018) 4142–4154.
[32] A. Bala, R. Sehrawat, A.K. Sharma, P. Soni, Synthesis and optical properties of polythiophene-capped ZnS/Mn quantum dots, J. Mater. Sci. - Mater. Electron. (2021).
[33] Y. Hao, L. Wang, B. Zhang, D. Li, D. Meng, J. Shi, et al., Manganese dioxide nanosheets-based redox/pH-responsive drug delivery system for cancer theranostic application, Int J Nanomed. 11 (2016) 1759–1778.
[34] L. Miao, L. Jiao, Q. Tang, H. Li, L. Zhang, Q. Wei, A nanozyme-linked immunosorbent assay for dual-modal colorimetric and ratiometric fluorescent detection of cardiac troponin I, Sens. Actuators, B 288 (2019) 60–64.
[35] D. Li, Y. Jiang, S. Chen, Q. Zhao, Y. Zhang, W. Wang, et al., A simple and sensitive assay of alkaline phosphatase activity in serum by fluorescent silicon nanoparticles based on inner filter effect, Sens. Actuators, B 307 (2020), 127589.
[36] Y. Han, Z. Ye, F. Wang, T. Chen, L. Wei, L. Chen, et al., Single-particle enumeration-based ultrasensitive enzyme activity quantification with fluorescent polymer nanoparticles, Nanoscale 11 (2019) 14793–14801.
[37] Z. Omran, T. Cailly, E. Lescot, J.S.D. Santos, J.H. Agondanou, V. Lisowski, et al., Synthesis and biological evaluation as AChE inhibitors of new indanones and thiaindanones related to donepezil, Eur. J. Med. Chem. 40 (2005) 1222–1245.
[38] M. Pistolozzi, H. Du, H. Wei, W. Tan, Stereoselective inhibition of human butyrylcholinesterase by the enantiomers of bambuterol and their intermediates, Drug Metabolism and Disposition 43 (2015) 344–352.
[39] J. Zhang, L. He, X. Zhang, J. Wang, L. Yang, B. Liu, et al., Colorimetric and SERS dual-readout for assaying alkaline phosphatase activity by ascorbic acid induced aggregation of Ag coated Au nanoparticles, Sens. Actuators, B 253 (2017) 839–845.

Yue Zhang is currently a PhD student in College of Chemistry, Jilin University. Her interest is spectral analysis.

Yanhua Wu gained her doctor's degree from College of Public Health, Jilin University in 2015 and she is an associated professor in Jilin University. Her research areas are epidemiology and bio-statistics.

Lin Liu is currently a PhD student in College of Chemistry, Jilin University. Her interest is chromatographic analysis.

Wei Wang is currently a B.S student in College of Chemistry, Jilin University. Her interest is spectral analysis.

Wei Zhang is currently a PhD student in College of Chemistry, Jilin University. Her interest is spectral analysis.

Daqian Song gained his doctor's degree from College of Chemistry, Jilin University in 2003 and he is a professor in that school. His research areas are spectral and chromatography analysis.

Xinghua Wang gained his doctor's degree from College of Chemistry, Jilin University in 2006 and he is a professor in that school. His research areas are spectral and chromatography analysis.

Rui Su gained her doctor's degree from College of Chemistry, Jilin University in 2012. Now, she is an engineer in Jilin University. Her research areas are anticancer components of Chinese Herbs and mass spectrometry analysis.